Journal of Organometallic Chemistry, 423 (1992) 415–430
Elsevier Sequoia S.A., Lausanne
JOM 22215

Chemistry of Pd^{II} complexes containing both BINAP (2'2'-bis(diphenylphosphino)binaphthyl) and a η^3-pinene or -allyl ligand. NMR studies on $[Pd(\eta^3\text{-}C_{10}H_{15})\{S(-)BINAP\}](CF_3SO_3)$. The crystal structure of $[Pd(\eta^3\text{-}C_{10}H_{15})(4,4'\text{-dimethylbipyridine})](CF_3SO_3)$

Christian J. Ammann, Paul S. Pregosin*, Heinz Rüegger
Laboratorium für Anorganische Chemie, ETH-Z, Universitätstrasse 6, CH-8092 Zürich (Switzerland)

Alberto Albinati, Francesca Lianza
Istituto di Chimica Farmaceutica, Università di Milano, Viale Abruzzi 42, I-20131 Milano (Italy)

and Roland W. Kunz
Organisch-Chemisches Institut der Universität Zürich, Winterthurerstrasse 190, CH-8057 Zürich (Switzerland)

(Received June 28, 1991)

Abstract

One and two-dimensional ^1H, ^{13}C and ^{31}P NMR studies on palladium(II) complexes containing η^3-$C_{10}H_{15}$ or η^3-C_4H_7 allyl and $S(-)$BINAP ligands are reported. Details of the three-dimensional solution structure for $[Pd(\eta^3\text{-}C_{10}H_{15})\{S(-)BINAP\}](CF_3SO_3)$ based on ^1H-2D NOESY and molecular modelling calculations are presented. The structure for the model β-pinene allyl complex $[Pd(\eta^3\text{-}C_{10}H_{15})(4,4'\text{-dimethylbipyridine})](CF_3SO_3)$ has been determined by an X-ray diffraction study, which reveals that the CH_2 terminal allyl carbon is significantly displaced from the N–Pd–N plane.

Introduction

2,2'-Bisdiphenylphosphinobinaphthyl, BINAP, continues to attract attention owing to the activity of its rhodium [1] and ruthenium [2] complexes in homogeneous catalysis. Despite the successful use of this ligand, in its optically active $R(+)$ and $S(-)$ forms, there have been few studies on the NMR characteristics of its complexes [1b], and none that compare the donating properties of this ligand with those of more frequently employed tertiary phosphines. In addition to learning about its electronic properties it would be useful to be able to map out the non-bonding interactions between a coordinated BINAP ligand and an organometallic ligand, e.g. a η^3-allyl. This is best achieved by use of Overhauser

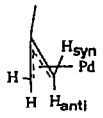

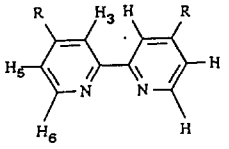

R=CH_3

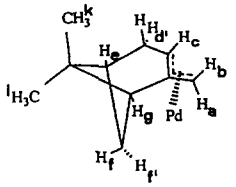

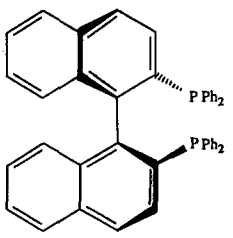

S(-)

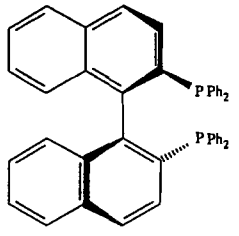

R(+)

Scheme 1

effects [3,4], and such experiments require a previous detailed knowledge of the ^1H NMR characteristics of the complex in question.

We present here:

i) ^{31}P, ^{13}C and ^1H NMR data for the complexes [Pd(η^3-C_4H_7){*S*(−)-BINAP}](CF_3SO_3), **1**, [Pd(η^3-$C_{10}H_{15}$){*S*(−)BINAP}](CF_3SO_3), **2**, and additional data for [Pd(η^3-$C_{10}H_{15}$){*R*(+)BINAP}](CF_3SO_3), **3**;

ii) 2D ^1H NOESY studies on **2** designed to elucidate aspects of the 3D solution structure;

iii) the crystal structure of the model η^3-$C_{10}H_{15}$ allyl complex [Pd(η^3-$C_{10}H_{15}$)-(4,4′-dimethylbipyridine)](CF_3SO_3), **4**;

iv) results of calculations directed towards understanding of the solution structure of **2**.

Results and discussion

NMR spectroscopy of 1

Schemes 1 and 2 depict the ligands under discussion and show positions of the phenyl groups that form the chiral pocket. In scheme 2 the complexes are viewed from behind the allyl ligand looking towards the palladium(II). The relative positions of the Ph groups with respect to the allyl are indicated by the abbreviated allyl with H^a, H^b and H^c shown. Since there is a substantial number of η^3-C_4H_7 palladium complexes [5–8] we begin our discussion with complex **1**.

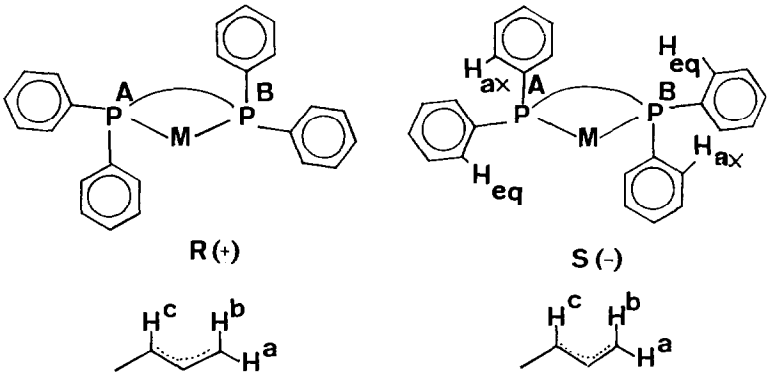

Scheme 2

The ^{31}P NMR of **1** at 101 MHz shows a tightly-coupled AB spectrum centered at $\delta = 22.9$, with ca. 1 Hz separation of the most intense lines. Even though the allyl is symmetrical the two phosphorus spins are non-equivalent (there are dynamic processes for allyl complexes that would allow rotation of the allyl but never average the two environments). Support for this asymmetry comes from the ^{13}C spectrum of **1** which reveals that there are non-equivalent terminal allyl carbons at $\delta = 79.0$ and 72.9. Consequently, we believe that this lower symmetry stems from the pseudo-equatorial and axial phenyl rings (see Schemes) which do not exchange positions. Åkermark and co-workers [9] have made a detailed study of the terminal methylene ^{13}C positions in a series of η^3-C_4H_7 π-allyl Pd^{II} complexes. They report higher field signals, ca. $\delta = 60$ for η^3-C_4H_7 *trans* to nitrogen ligands and lower field signals when the allyl is *trans* to a tertiary phosphine, e.g., $\delta = 70.4$ for $[Pd(\eta^3\text{-}C_4H_7)(Ph_2PCH_2CH_2PPh_2)]^+$ and $\delta = 78.55$ for $Pd(\eta^3\text{-}C_4H_7)(PPh_3)_2]^+$. For purposes of comparison we prepared the model complex $[Pd(\eta^3\text{-}C_4H_7)(Me_2PCH_2CH_2PMe_2)](CF_3SO_3)$, and found for this compound $\delta^{31}P = 30.3$, $\delta^{13}CH_2(allyl) = 65.8$. Since this methylphosphine chelate is expected to be a good donor, perhaps the presence of small substituents on phosphorus is partially responsible for the relatively high field allyl CH_2 carbon resonance. In any case, based on the ^{13}C-allyl data for **1**, *S*(−)BINAP shows no unusual electronic characteristics relative to those of PPh_3 or $Ph_2PCH_2CH_2PPh_2$.

The ^1H NMR spectrum of the allyl of **1** shows four allyl protons at 3.96, 3.74, 3.60 and 3.07 ppm, respectively, plus the CH_3 signal at $\delta = 1.98$. A two-dimensional ^{13}C, ^1H correlation allows us to attribute the two protons at $\delta = 3.96$ and 3.60 to the low field carbon and the two at 3.74 and 3.07 to the high field methylene allyl carbon. We can identify the *syn* protons (via Overhauser enhancements from the CH_3) at $\delta = 3.60$ and 3.74; consequently, it is the *anti* protons that are markedly different [10]. In view of the similar ^{31}P chemical shifts, we believe that the 0.89 ppm difference in these *anti* protons stems from anisotropic effects. We assign the *anti* proton adjacent (*cis*) to P^A (see Schemes) to the resonance at $\delta = 3.96$ (and thus the carbon at $\delta = 79.0$ as *cis* to P^A) on the basis of the discussion for **2** and **3** below.

The NMR spectra for complex **2** are, not surprisingly, more complicated owing to the lower symmetry and different electronic properties of the η^3-$C_{10}H_{15}$,

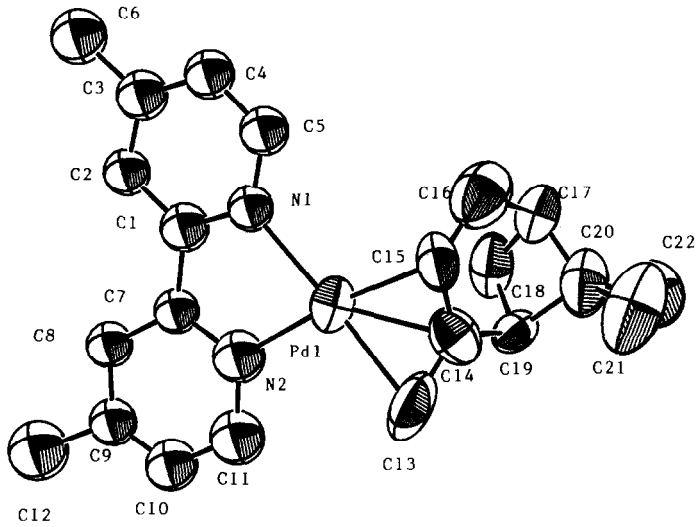

Fig. 1. ORTEP view of **4**.

β-pinene allyl fragment. This allyl ligand has been used previously [8,11,12], and we thought it would be helpful to have a more exact knowledge of this moiety. To this end we determined the structure * of the complex [Pd(η^3-$C_{10}H_{15}$)(4,4'-dimethylbipyridine)](CF_3SO_3), **4**.

Molecular structure of 4

The molecular structure of **4** was determined by X-ray diffraction and an ORTEP view of one of the two independent molecules in the cell is shown in Fig. 1. The immediate coordination sphere consists of the bipyridyl and the β-pinene allyl ligands around the Pd^{II} centre. The $CF_3SO_3^-$ anion was located, and is present as a discrete species remote from the metal centre. The two independent molecules in the unit cell are equivalent within experimental error. The bondlengths and angles provided in the following discussion are mean values. Two interesting features associated with this structure are pertinent for our purposes.

1) The plane of the allyl ligand, defined by C(13), C(14) and C(15), makes an angle of 118 ± 2° with respect to the plane defined by Pd–N(1) and N(2), with the C(14)–C(19) vector pointing away from the palladium.
2) Relative to a coordination plane containing Pd, N(1) and N(2) the allyl is situated so that the CH_2, C(13), is out of the plane, C(14) is out of the plane in an opposite direction, and C(15) lies close to the plane.

Table 1 shows selected bond lengths and angles for the complex, and Tables 2 and 3 give positional parameters and experimental details, respectively. The Pd–N separations are normal [13–16], with Pd–N(1) slightly longer than Pd–N(2). The Pd–C(allyl) separations are all similar and as expected [13,16–18] averaging 2.16(4)

* Attempts to prepare suitable crystals of the BINAP complexes gave unsatisfactory results. We think that the structure for **4** is informative with respect to the electronic properties of the allyl ligand since the bipyridyl ligand is relatively small.

Table 1

Selected bond lengths (Å) angles (deg) and torsion angles (deg) for compound **4** (the two sets of numbers refer to the two independent molecules in the unit cell)

Pd(1)–N(1)	2.14(1)	2.14(1)
Pd(1)–N(2)	2.10(1)	2.03(2)
Pd(1)–C(13)	2.13(2)	2.22(2)
Pd(1)–C(14)	2.19(2)	2.14(2)
Pd(1)–C(15)	2.17(2)	2.10(2)
C(1)–C(7)	1.48(2)	1.49(2)
N(1)–C(1)	1.37(2)	1.28(2)
N(1)–C(5)	1.29(2)	1.34(2)
N(2)–C(7)	1.32(2)	1.35(2)
N(2)–C(11)	1.38(2)	1.42(2)
C(13)–C(14)	1.48(3)	1.37(3)
C(14)–C(15)	1.36(3)	1.39(2)
N(1)–Pd(1)–N(2)	77.5(5)	76.6(6)
Pd(1)–N(1)–C(1)	112.1(8)	116.2(1.0)
Pd(1)–N(1)–C(5)	127.6(1.0)	125.5(1.0)
Pd(1)–N(2)–C(7)	117.8(1.0)	117.6(1.0)
Pd(1)–N(2)–C(11)	123.2(1.0)	123.6(1.0)
C(13)–C(14)–C(15)	111.8(2.0)	123.0(2.0)
C(13)–C(14)–C(19)	125.9(2.0)	121.0(2.0)
C(15)–C(14)–C(19)	121.5(2.0)	114.5(2.0)
N(1)–C(1)–C(7)–N(2)	1.0(2.0)	0.0(3.0)

Å. The bond angles within the bipyridyl are those expected for an aromatic hydrocarbon. The C(1)–C(7) bond length of 1.48(2) Å is suggestive of a single bond, and the torsion angle N(1)–C(1)–C(7)–N(2) is close to 0°.

It is recognized [16–18] that the allyl plane makes an angle of $> 90°$ with the coordination plane, and values from ca. 100–121° are known [19], and the value of $118 \pm 2°$ for **4** lies at the upper end of this range. When account is taken also of the observed position of the allyl ligand, i.e., C(13) is out of the N(1)–Pd–N(2) plane, it seems that the β-pinene allyl takes up a position with respect to the metal such as to optimize overlap of the various allyl orbitals with the Pd^{II}. We consider that this is an interesting distortion, and note that it is not a consequence of the size of the bipyridyl, which does not approach the allyl to any significant extent (C(5)–C(15) > 3.6 Å, C(11)–C(13) > 3.5 Å). This allyl distortion plays a part in the subsequent discussion of the solution structure.

^{31}P and ^{13}C NMR spectroscopy for 2 and 3

In the *S*(−)BINAP complex, **2**, the two ^{31}P spins are non-equivalent and appear as an AX spin system at $\delta = 27.5$ (P^B) and 22.9 (P^A), $^2J(P,P) = 50$ Hz. In the *R*(+) isomer, **3**, the corresponding values are 22.8 (P^B) and 19.6 (P^A) ppm, with $^2J(P,P) = 52$ Hz. Consequently the ^{31}P chemical shift data are suggestive of differences in bonding between the two diastereomers. The allyl carbons for **2** and **3** are found at 81.3 and 73.4 ppm, and 86.4 and 74.5 ppm, respectively, with the ^{13}CH at lower field than $^{13}CH_2$. For the CH_2 these values are consistent with our ^{13}C results for **1**. For both **2** and **3** the allyl ^{13}C positions are to low field of the corresponding allyl signals in **4**, $\delta CH = 67.5$, $\delta CH_2 = 60.0$, as expected on the

Table 2

Positional parameters and their estimated standard deviations

Atom	x	y	z	B (Å^2)
Pd1	0.3647(2)	0.426	0.7270(2)	5.29(4)
Pd2	0.3190(2)	0.2368(1)	0.1794(1)	5.44(4)
S1	0.2807(7)	0.9197(4)	0.5179(5)	5.9(1) *
S2	0.2636(8)	0.7539(4)	0.0287(6)	6.7(2) *
F1	0.080(2)	0.985(1)	0.600(2)	11.0(6) *
F2	0.285(3)	0.995(2)	0.671(2)	14.5(8) *
F3	0.233(3)	1.043(1)	0.546(2)	13.1(7) *
O1	0.433(2)	0.937(1)	0.517(2)	10.3(6) *
O2	0.263(2)	0.861(1)	0.572(2)	9.4(6) *
O3	0.192(2)	0.926(1)	0.425(2)	10.0(6) *
O4	0.221(3)	0.815(2)	0.062(2)	12.7(8) *
O5	0.407(3)	0.748(2)	0.030(2)	11.6(7) *
O6	0.173(3)	0.733(2)	−0.059(2)	11.8(7) *
N1′	0.243(2)	0.5159(8)	0.712(1)	3.3(3)
N1	0.442(2)	0.1927(9)	0.310(1)	4.5(4)
N2′	0.457(2)	0.479(1)	0.855(1)	4.9(4)
N2	0.235(2)	0.144(1)	0.180(2)	6.1(5)
Cf1	0.222(3)	0.980(2)	0.581(2)	8.1(8) *
C1	0.414(2)	0.132(1)	0.325(2)	5.2(5) *
C1′	0.301(2)	0.563(1)	0.780(2)	4.1(4) *
Cf2	0.229(7)	0.704(3)	0.128(4)	17 (2) *
C2′	0.245(2)	0.626(1)	0.776(2)	4.6(5) *
C2	0.483(2)	0.096(1)	0.409(2)	4.9(5) *
C3′	0.130(3)	0.649(1)	0.702(2)	5.5(5) *
C3	0.591(3)	0.129(1)	0.471(2)	5.8(5) *
C4′	0.068(3)	0.593(1)	0.637(2)	5.1(5) *
C4	0.619(3)	0.192(1)	0.455(2)	5.4(5) *
C5′	0.132(3)	0.530(1)	0.646(2)	5.2(5) *
C5	0.544(3)	0.223(1)	0.375(2)	5.3(5) *
C6	0.667(3)	0.089(2)	0.561(2)	7.0(7) *
C6′	0.069(3)	0.715(1)	0.693(2)	5.6(6) *
C7′	0.420(2)	0.542(1)	0.861(1)	3.3(4) *
C7	0.296(2)	0.102(1)	0.253(2)	4.6(5) *
C8	0.245(2)	0.035(1)	0.254(2)	4.9(5) *
C8′	0.477(3)	0.580(1)	0.931(2)	5.4(5) *
C9′	0.590(3)	0.558(1)	1.011(2)	5.6(5) *
C9	0.133(3)	0.017(1)	0.182(2)	5.2(5) *
C10′	0.635(3)	0.494(1)	1.008(2)	5.9(6) *
C10	0.071(3)	0.056(1)	0.115(2)	6.2(6) *
C11′	0.566(2)	0.454(1)	0.926(2)	5.2(5) *
C11	0.118(3)	0.121(2)	0.108(2)	6.8(6) *
C12′	0.656(4)	0.602(2)	1.097(2)	8.5(8) *
C12	0.089(3)	−0.058(2)	0.190(2)	8.6(8) *
C13	0.221(4)	0.281(2)	0.035(2)	8.1(8)
C13′	0.503(3)	0.342(2)	0.714(2)	7.3(7)
C14	0.253(3)	0.329(1)	0.105(2)	6.0(6)
C14′	0.353(3)	0.323(1)	0.672(2)	6.2(6)
C15	0.391(2)	0.334(1)	0.164(2)	5.7(6)
C15′	0.296(3)	0.364(1)	0.596(2)	5.8(6)
C16′	1.136(3)	1.348(2)	1.554(3)	8.3(9)
C16	1.417(4)	1.381(2)	1.236(3)	9.0(9)
C17	1.261(4)	1.417(2)	1.259(2)	8.7(9)

Table 2 (continued)

Atom	x	y	z	B(Å^2)
C17′	1.082(3)	1.296(2)	1.617(3)	8.3(9)
C18′	1.123(3)	1.312(2)	1.721(2)	7.0(7)
C18	1.184(3)	1.439(2)	1.165(2)	8.0(8)
C19	1.124(2)	1.371(1)	1.147(2)	4.5(5)
C19′	1.262(3)	1.274(1)	1.715(2)	6.4(7)
C20	1.141(3)	1.365(1)	1.256(2)	7.2(7)
C20′	1.184(3)	1.237(2)	1.630(2)	7.3(7)
C21	1.052(3)	1.490(2)	1.179(3)	9 (1)
C21′	1.100(4)	1.175(2)	1.659(3)	9.7(9)
C22	1.258(3)	1.475(2)	1.071(3)	11 (1)
C22′	1.264(3)	1.218(1)	1.541(2)	6.4(7)
F4	0.263(3)	0.642(1)	0.108(2)	13.8(7) *
F5	0.298(3)	0.716(1)	0.208(2)	14.6(7) *
F6	0.090(3)	0.701(1)	0.131(2)	12.8(6) *

Atoms marked with a star were refined isotropically. Anisotropically refined atoms are given in the form of the isotropic equivalent displacement parameter defined as: $\frac{4}{3}[a^2B_{1,1} + b^2B_{2,2} + c^2B_{3,3} + (ab \cos \gamma)B_{1,2} + (ac \cos \beta)B_{1,3} + (bc \cos \alpha)B_{2,3}]$.

bases of Åkermarks data [9]. Consequently, for our η^3-$C_{10}H_{15}$ allyl complex, as well as for the methallyl complex **1**, introduction of a chelating diphosphine, e.g. BINAP, in place of a nitrogen chelate results in significant changes in the electronic structure of the allyl moiety. For the model complex [Pd(η^3-$C_{10}H_{15}$)($Me_2PCH_2CH_2PMe_2$)](CF_3SO_3), the terminal allyl carbons appear at 77.4 (CH) and 61.8 (CH_2), with the latter values again at rather high field.

1 and 2D ^1H NMR spectroscopy for 2

Our interest in the ^1H characteristics of **2** stems from our wish to define the relative positions of sections of the BINAP, and specifically the two PPh_2 moieties, relative to the β-pinene allyl. This requires us to find and (if possible) unequivocally assign the *ortho* protons H_{eq} and H_{ax} (see Scheme 2). Previous experience [12] with the β-pinene allyl η^3-$C_{10}H_{15}$ suggested that we begin with a $^{31}P,^1H$ two-dimensional correlation, and we show sections of this in Figs. 2 and 3. The reasoning is as follows: it is known [20,21] that spin–spin coupling constants from an allyl proton to a ^{31}P spin *trans* are relatively large, and so a $^{31}P,^1H$ correlation will connect the allyl protons H^a and H^b to P^A and H^c to P^B. The same spectrum connects each ^{31}P spin to the three aryl proton types *ortho* to this donor atom; H(3) of the binaphthyl and H_{eq} and H_{ax} of the PPh_2 moieties. In addition to revealing these six aromatic protons, Fig. 3 has an unexpected feature in that: one of the cross peaks for P^A (δ ca. 7.2, upper cross peaks) correlates to a very broad resonance. Lowering the temperature to 223 K confirms that one ring is involved in a relatively slow dynamic process, presumably, rotation around the P^A–C_{ipso} bond. This was not the case for the analogous *R*(+) isomer. We assign this ring as P^A_{ax} on the basis of the Overhauser effects discussed below and the relatively high field shifts at 223 K for the protons of this ring (e.g., H^A_{ax} moves upfield by ca. 0.7 ppm to $\delta = 6.5$ and another proton, probably one in *meta* position, changes from ca. $\delta = 6.6$ to 6.0). We believe that these high field displacements arise from ring

Table 3

Experimental data for the X-ray diffraction study of **4**

Formula	$C_{23}H_{28}F_3N_2O_3PdS$
Molecular weight	575.954
Crystal size, mm	0.50×0.20×0.15
Data collection temperature, °C	23
Crystal system	Monoclinic
Space group	$P2_1$
a, Å	9.271(5)
b, Å	20.205(2)
c, Å	13.487(2)
β, deg	98.67(1)
V, Å^3	2497.4(9)
Z	4
ρ(calcd), g cm^{-3}	1.550
μ, cm^{-1}	8.716
Radiation	Mo-K_α, graphite monochromated, $\lambda = 0.71069$
Measured reflections	$\pm$h, +k, +l
θ range, deg	$2.5 < \theta < 25.0$
Scan type	$\omega/2\theta$
Scan width, deg	1.10+0.35 tan θ
Counting time, max, s	70
Time bkgd, s	0.5 * scan-time
Scan speed, max, deg/min	5.1
Prescan rejection limit	0.55(1.82σ)
Prescan acceptance limit	0.025(40.00 σ)
Horiz. receiving slit, mm	1.70+tan θ
Vert. receiving slit, mm	4.0
No. data collected	3241
No. observed reflections (n_o) ($\|F_o\|^2 > 3.0\sigma(\|F\|^2)$)	2510
Transmission factors	0.9985–0.9173
No. of parameters refined (n_v)	351
R; R_w	0.065; 0.076
G.O.F.	2.189

$R = \Sigma \| F_o | - 1/k | F_o \| / \Sigma | F_o |$; $R_w = [\Sigma w(|F_o| - 1/k|F_o|)^2 / \Sigma w |F_o|^2]^{1/2}$ where $w = [\sigma^2(F_o)]^{-1}$ and $\sigma(F_o) = [\sigma^2(F_o^2) + f^2(F_o^4)]^{1/2}/2F_o$ with $f = 0.070$; G.O.F. $= [\Sigma w(|F_o| - 1/k|F_o|)^2/(n_o - n_v)]^{1/2}$.

current effects associated with the naphthyl moiety. We return to this point after presentation of the calculated structure.

The assignment of the remaining aliphatic β-pinene protons follows from ^{1}H-COSY [22], previous experience [12], NOE's, and consideration of coupling constants. We avoid attempting to use ^{1}H chemical shifts in the assignment, since these can be deceptive. Selected room temperature ^{1}H positions for our complexes are shown in Table 4. A comparison of the allyl ^{1}H resonances for the $S(-)$ and $R(+)$ isomers, **2** and **3**, respectively, reveals very marked, not yet understood changes, e.g. $\Delta\delta$ (δ = complex **2** − δ complex **3**) for: $H^a = +0.57$, $H^b = -0.75$, $H^c = +0.91$. Since the allyl ^{13}C shifts, especially for the CH_2 carbons, are similar, we assume that these $\Delta\delta$ values arise from anisotropic effects and specifically the placement of the axial phenyl groups. The axial phenyl groups are expected from crystallographic studies [2b] to spend most of their time parallel to the naphthyl

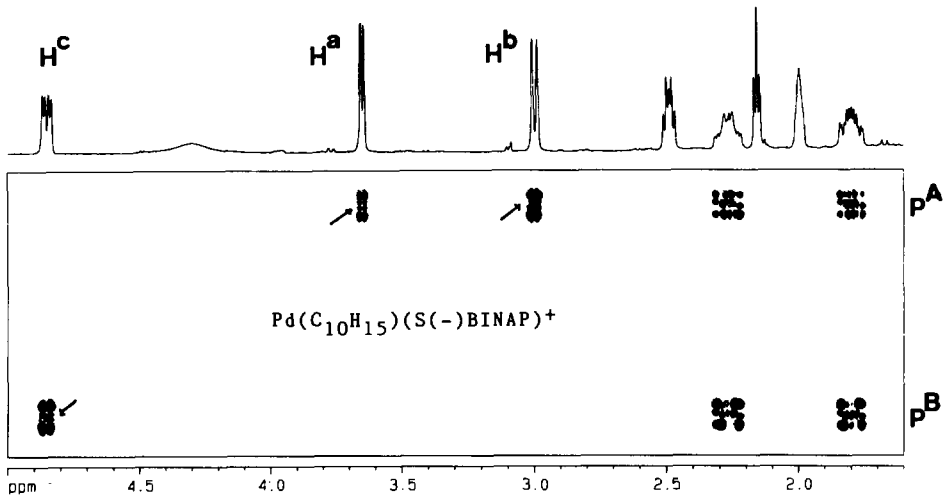

Fig. 2. Section of the $^{31}P,^{1}H$ correlation for **2** showing the allyl protons of the pinene allyl. The upper cross-peaks arise from spin–spin coupling to P^A, the lower to P^B.

rings. This places proton H^b in a deshielding region [23] in the *R*(+) isomer **3** and H^a and H^c in deshielding regions in the *S*(−) isomer **2**. This ring current effect also accounts for the low field 3.96 value, for the *anti* proton of the *S*(−) complex **1**, and permits us to complete the assignment of the four allyl signals in **1**.

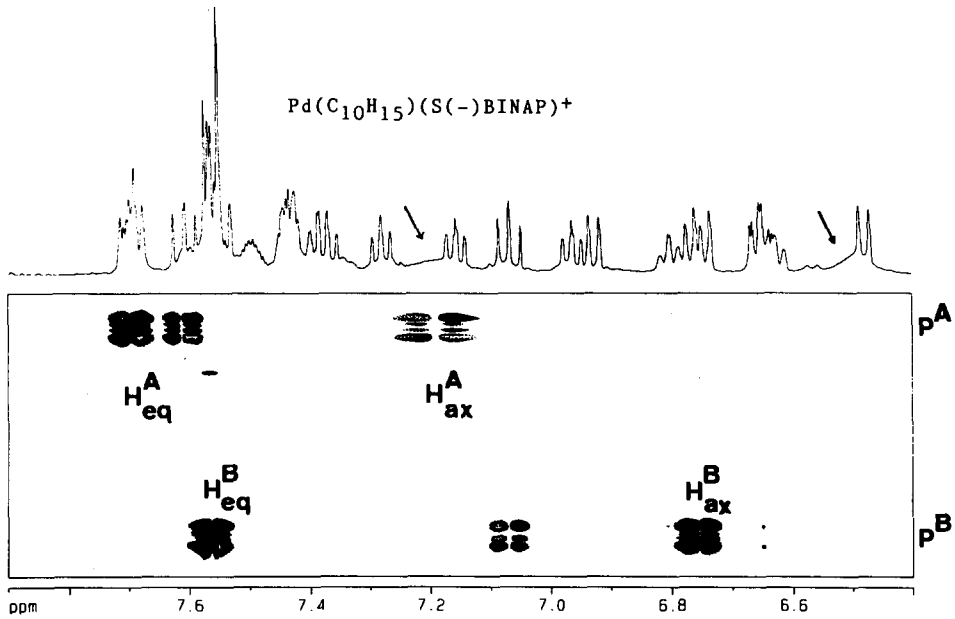

Fig. 3. Section of the $^{31}P,^{1}H$ correlation for **2** showing the aryl protons. There are three sets of cross-peaks from each of the two phosphorus spins. Note that one of the cross-peaks, that arising from H^A_{ax}, is broad (see arrow, and text).

Table 4

Selected NMR data [a] for **1–3**

	1 [b]		**2** [c]	**3** [d]
^{31}P	22.9	P^A	22.9	19.6
terminal allyl		P^B	27.5	22.8
^{13}C	79.0	CH	81.3	86.4
	72.9	CH_2	73.4	74.5
^1H	3.60	a	3.66	3.09
	3.96	b	3.01	3.76
	3.07	c	4.87	3.96
	3.74	d	2.32	1.60
		d′	1.81	0.85
		e	2.01	1.80
		f	2.50	2.55
		f′	1.20	1.66
		g	2.17	2.12
		CH_3 [e]	1.02	0.86
			1.29	1.24
		H^A_{eq}	ca 7.67 [c]	7.69
		H^A_{ax}	ca 7.16 [c]	7.05
		H^B_{eq}	ca 7.57 [c]	7.43
		H^B_{ax}	ca 6.75 [c]	7.28

[a] $CDCl_3$, room temperature. For **4**: $^{13}CH_2$, 60.8; ^1H:H_{syn}, 4.24; H_{anti}, 3.47. [b] See text for details of assignment, $\delta(^{31}P)$ is centre of the AB spectrum. [c] The *ortho* PPh_2 overlap with other aryl signals so the chemical shifts are not very exact. The r.t. value for H^A_{ax} is given, see text. 600 MHz, $CDCl_3$, ^1H data. [d] 500 MHz, $CDCl_3$ ^1H data. [e] Low field CH_3 signal is proximate to that of allyl.

The assignment of the individual H_{eq} and H_{ax} protons follows from the analysis of the ^1H-2D NOESY spectrum of **2**, one section of which is shown in Fig. 4. Molecular models and modeling studies (see below) make it obvious that the equatorial rings come close to the allyl *anti* protons, whereas one of the axial phenyl rings is close to $H^{f'}$ and perhaps the *syn* proton H^a. Since the ^{31}P spins are assigned, it is possible to identify the various portions of the complex. Specifically the NOEs from H^c and H^b to the aryl protons at δ = ca. 7.70 and 7.57 identify the H^A_{eq} and H^B_{eq} protons, respectively, despite the fact that these are partially or completely overlapped by other resonances. Strong NOEs from H^a, $H^{f'}$ and H^g to the aryl resonance at δ = 6.76 identifies H^B_{ax}. There are no strong NOEs from H^A_{ax} to the allyl.

The results of these detailed NMR studies allow us to draw a few qualitative conclusions. First, we can differentiate between the two diastereomeric complexes **2** and **3** and assign their structures by use of NOE data. This assignment arises due to the different non-bonded contacts between the two ligands in these complexes. Recognizing these contacts is important since it may help us to understand why one section of one of the ligands is more accessible than the other. Specifically, it is now clear that there is a special geometric relationship between the allyl carbons and individual phenyl rings of the BINAP. In addition, we can specify which of these rings is relatively close to the remaining sections of the hydrocarbon. A comparison of the NOE data from the two complexes **2** and **3** reveals subtle differences in the relative disposition of the allyl and BINAP ligands relative to

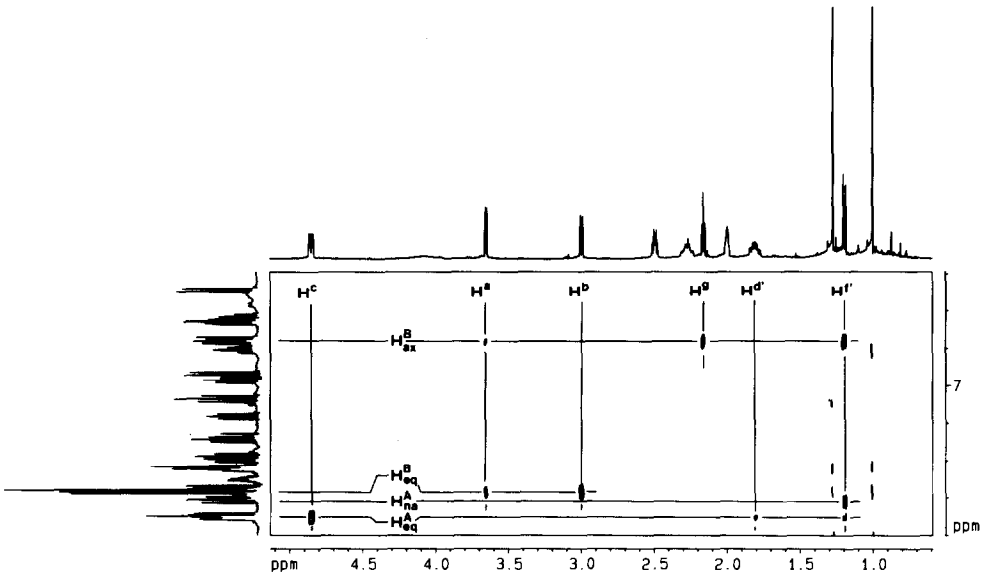

Fig. 4. Section of the ^{1}H 2-D NOESY for **2** showing the key cross-peaks which relate the protons on the PPh_2 moieties to the various allyl protons.

one another. In order to understand more fully possible sources for these differences we carried out some simple calculations.

Calculations for 2

Using the crystallographic literature for complexes of BINAP [2b,24–26] and for allyl complexes in general [27] together with our determination of the structure of **4** we attempted to model **2** by use of the program MM2(87) [28]. This type of calculation assumes that non-bonded interactions play a major role in the overall structure. To the extent that this is true, such effects are well reproduced by MM2(87) providing that the program can be suitably parametrized. The bond-lengths and angles, chosen as input, are based on the values in the literature, and we have selected 118° as the angle between the P–Pd–P and allyl carbon plane. There is no NOE NMR input. The lowest energy structure, shown in Fig. 5, has several interesting features not observed in our earlier study [12] for **3**, the *R*(+) isomer. It predicts: 1) a short contact from $H^{d'}$ to H^A_{eq}; 2) a short contact from $H^{f'}$ to the *ortho* BINAP proton of the naphthyl attached to P^A and; 3) a rather long separation between the "dynamic" H^A_{ax} and the *anti* protons, H^b and H^c (ca. 3.4 Å, see Table 5). In contrast to the findings for **3** [12], the calculation reveals an acceptable energy minimum without substantial rotation of the allyl plane with respect to the P–Pd–P plane. Further, the CH allyl carbon is found ca. 0.16 Å below the P–Pd–P plane (viewed from behind the allyl towards the Pd as before); however, the allyl CH_2 carbon is now roughly in the P–Pd–P plane, in contrast to our X-ray data for **4**.

The above predictions have all been confirmed independently via observations of the presence or absence of NOE's. We find a strong NOE from H^d to H^A_{eq} (this was very weak in **3**), a strong NOE from $H^{f'}$ to the *ortho* BINAP proton

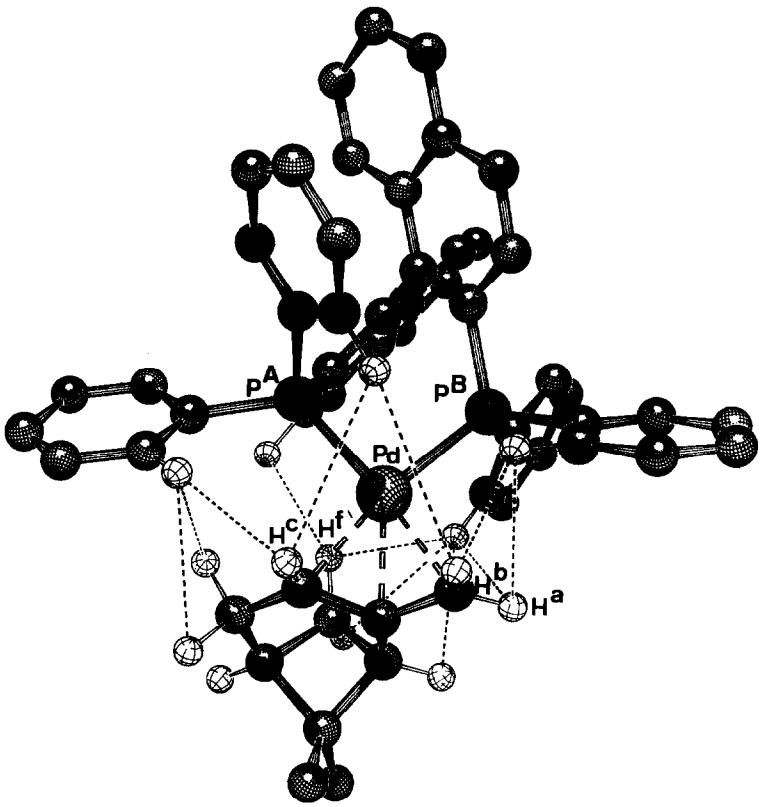

Fig. 5. Structure calculated for **2** using MM2. Note the parallel relation of the axial rings with the naphthyl moieties, the various close contacts of the equatorial P^B ring to the allyl and the close contact of the naphthyl proton to $H^{f'}$.

associated with P^A (absent in **3**), and no NOE from H^A_{ax} to the allyl (but a strong NOE from H^A_{ax} to $H^{f'}$ in **3**). Allowing for its shortcomings (such as electronic effects not being considered) the model seems to have some validity.

Table 5

Calculated distances between the PPh_2 *ortho* protons and selected β-pinene allyl protons

	PPh_2	β-pinene	distance, Å
1	H^B_{ax}	$H^{f'}$	2.3
2	H^B_{ax}	H^g	2.7
3	H^B_{ax}	H^a	3.1
4	H^B_{eq}	H^a	3.3
5	H^B_{eq}	H^b	2.2
6	H^A_{ax}	H^b	3.4
7	H^A_{ax}	H^c	3.4
8	H^A_{eq}	H^c	2.3
9	H^A_{eq}	$H^{d'}$	2.6
10	H^B_{ax}	H^f	2.9
11	H^A_{BINAP}	$H^{f'}$	2.5

In view of the experimentally observed slow rotation of one ring in **2** we have calculated the barriers to P–C (aryl) rotation about the four P–C bonds in the two PPh_2 moieties. For **2** and **3** we find the two activation energies for the equatorial ring rotation to be similar, as are the two energies for the axial P–Ph groups, but the former is ca. 50% smaller than the latter. Consequently, it is conceivable that one axial ring rotation may be slower. One interesting difference between **2** and **3** arising from the calculations concerns the equatorial P^A phenyl ring. This comes closer to the allyl hydrocarbon in **2**, and this explains the shorter $H^{d'}$, H^A_{eq} contact and perhaps also the higher activation energy for rotation of ring P^A_{eq} if it is assumed that both P^A rings are twisted away from the allyl. The calculations also suggest a slightly shorter separation of ring P^A_{ax} from the naphthyl in **2** (ca. 3.05 Å) relative to **3** (ca. 3.10 Å).

Conclusions

Despite its shortcomings, our approach to identifying aspects of the solution structures of **2** and **3** has produced new insights. The PPh_2 groups do encroach on the allyl, and to different extents in **2** and **3**. The contact is such that differences in dynamics and ^{13}C and ^{31}P shifts are observable. The X-ray structure of **4** serves as a reminder of the shortcomings of our calculation, since the solid-state data suggest electronic effects may be important. These electronic effects can produce rotations and other displacements of the allyl in the attempt to optimize its overlap with the palladium orbitals. If the CH_2 allyl were allowed to drop below the P–Pd–P plane and the allyl CH to move up, so that the distortion in **4** were present in **2**, the P^A_{eq} ring might be moved away from its already crowded position. This movement might, in turn, push the P^A_{ax} ring even closer to the naphthyl, thereby increasing the activation energy for rotation. In any case, the calculation predicted certain less than obvious contacts, e.g., between a binaphthyl proton and the allyl, which we were able to confirm. Taken together our data provide a reasonable picture of the solution structure of **2**. Clearly, the combined use of NOE's and calculations warrants further investigation.

Experimental

Preparation of 2 and 3

To a solution of $[Pd(\mu\text{-}Cl)(\eta^3\text{-}C_{10}H_{15})]_2$ (29.7 mg, 0.05 mmol) in 5 ml of methanol was added solid BINAP (66.7 mg, 0.11 mmol) and the resulting suspension stirred for 5 min to afford a light yellow solution. Addition of $[Tl(CF_3SO_3)]$ (37.9 mg, 0.11 mmol) results in immediate precipitation of TlCl.

After stirring for an additional 5 min the suspension was filtered through Celite and the solvents removed. The colourless oil which resulted was treated with ether to induce solidification of a solid. Removal of the ether gave the product in 92% (**2**) and 88% (**3**) yield. Complex **1** was prepared analogously.

The complexes $[Pd(\eta^3\text{-}C_4H_7)(Me_2PCH_2CH_2PMe_2)](CF_3SO_3)$, **5**, and $[Pd(\eta^3\text{-}C_{10}H_{15})(Me_2PCH_2CH_2CH_2PMe_2)](CF_3SO_3)$, **6**, were prepared as described above. The former was isolated as a colourless oil in 85% yield and was stable in solution. The latter proved to be unstable in solution and decomposed completely within a period of 12 h. For **5**: ^{31}P NMR, 30.3; ^{13}C NMR: (allyl CH_2) 65.8, J(C,P)

17 Hz, (allyl C) 137.1, J(P,C) 6 Hz, (CH_3) 24.6, (PCH_2) 28.4, J(P,C) 23 Hz; (PCH_3) 14.5, J(P,C) 13 Hz; (PCH_3) 15.4, J(P,C) 13 Hz. For **6**: ^{13}C NMR, (allyl CH_2) 61.8, J(P,C) 26 Hz; (allyl CH) 77.4, J(P,C) 32 Hz; (allyl C) 145.0, J(P,C) 4 Hz; (PCH_2) 27.8, 28.4; (PCH_3) 11.0, 12.9. ^1H NMR (H^a) 3.88, J(P,H) 6, 2 Hz; (H^b) 2.70 (J(P,H) 11 Hz; (H^c) 3.96, J(P,H) 11 Hz, 5 Hz; (PCH_3) 1.41, 1.58, 1.66, 1.68.

Crystallography

Crystals suitable for X-ray diffraction of compound **4** were obtained with some difficulty by recrystallization from chloroform/THF solution. They are stable in air. A small elongated prismatic crystal was found to be suitable for the data collection (even though scattering only weakly) and was mounted on a glass fibre at a random orientation. An Enraf–Nonius CAD4 diffractometer was used for the unit cell and space group determination and for data collection. Unit cell dimensions were obtained by least squares fit of the 2θ values of 25 high order reflections ($9.3° < \theta < 17.8°$) using the CAD4 centring routines. Selected crystallographic and other relevant data are listed in Table 3. Data were measured with variable scan speed to ensure constant statistical precision on the collected intensities. Three standard reflections (0 8 5; 0 4 6; 0 $\bar{4}$ $\bar{6}$) were used to check the stability of the crystal and of the experimental conditions and measured every hour; no significant variation was detected. The orientation of the crystal was checked by measuring three reflections every 300 measurements. Data were corrected for Lorentz and polarization factors and for decay, using the data reduction programs of the CAD4 SDP package [29]. An empirical absorption correction was applied by using azimuthal (ψ) scans of four "high-χ" angle reflections ($\chi > 85.6°$; $9.0° < \theta < 16.0°$). The standard deviations on intensities were calculated in terms of statistics alone, while those on F_o were calculated as reported in Table 3. Intensities were considered as observed if $|F_o^2| > 3.0\sigma|F^2|$, and used for the solution and refinement of the structure. A value F_0 of 0.0 was given to those reflections having negative net intensities. The structure was solved by a combination of direct and Fourier methods and refined by full matrix least squares [29] (the function minimized was $[\Sigma w(|F_o| - 1/k(|F_c|)^2])$ with $w = [\sigma^2(F_o)]^{-1}$. No extinction correction was necessary. The scattering factors used, corrected for the real and imaginary parts of the anomalous dispersion, were taken from the literature [30]. Anisotropic temperature factors were used for the Pd atom and the carbon atoms of the β-pinene moiety. A refinement including anisotropic temperature factors for all atoms did not improve significantly (as based on Hamilton's test [31]) the agreement factors. A model with all the ligand atoms treated isotropically gave a significantly worse agreement. The counterions were found to be slightly disordered, as were for the β-pinene ligand. This and the weakness of the reflections may account for the limited precision of the structural parameters. The hydrogen atoms were included in their idealized positions (C–H = 0.95 Å, $B = 1.3 \times B$ of the bonded atoms) but not refined. Upon convergence the final Fourier difference map showed no significant feature. All calculations were carried out with the SDP crystallographic package [29]. The handedness of the crystal was checked by Hamilton test [31,32]. Final atomic coordinates and equivalent thermal factors are given in Table 2. A list of calculated and observed structure factors, extended list of bond lengths, angles and torsion angles is available from the authors.

Molecular modelling

MM2(87) was used with its standard features [28]. (A complete list of constants is available from the authors as supplementary material.) Palladium was assigned to atom type 32 and the two phosphorus and terminal allyl carbon types to atoms 25 and 26 (P's) and 48 and 49 (C's) respectively. This assignment was necessary to treat the *cis/trans* relationships properly. The structural characteristics of the computed structure are consistent with what one would expect [24–27]. Specifically: Pd–P 2.34 Å; P–Pd–P 90.9°; P–C, 1.87 Å; Pd–P–C 107–119°; Pd–C(allyl) 1.44 Å; C–C–C angle for the three allyl carbons 120.3°, and the angle between the P–Pd–P and allyl carbons plane 118°. The following structures from the Cambridge Crystallographic Database were used as a basis: bnaprh, datzon, fuxsum, gahyap, japxaz, bicloo, sayhef, alanpd, busvug, docwef and saygee (P–M–P); aombpd, deyhiy, bodwia, cajjom, cawler, cekkos, bexhiv, bilhej, bodwew, dulrux, fidrix, fidrod, mapicp, mmchpd, npalpd, npalpe, tbbmap, xprgpd (M-allyl environment). No NOE constraints were used to bias the packing.

NMR spectra were recorded from $CDCl_3$ solutions in sealed 5 mm (o.d.) tubes on Bruker AC250, AMX500 and AMX600 spectrometers operating in the Fourier transform mode at 250.13 (101.3, 62.9), 500.13 (202.5, 125.8) and 600.13 (243.0, 150.9) MHz for ^{1}H, ^{31}P and ^{13}C, respectively. Standard pulse schemes were employed for 'inverse' $^{31}P-^{1}H$ [34] and $^{13}C-^{1}H$ [35] heteronuclear correlations. The ^{1}H–2D-NOESY [36] spectra were obtained with a mixing time $\tau_{mix} = 800$ msecs.

Acknowledgements

PSP thanks the ETH and the Swiss National Science Foundation for support and Johnson-Matthey for the loan of $PdCl_2$. A.A. thanks the Italian CNR for support. We also thank Dr. Detlef Moskau and Spectrospin AG for AMX-600 measurements.

References

1 (a) R. Noyori, Chimia, 42 (1988) 215; (b) S. Inoue, H. Takaya, K. Tani, S. Otsuka, T. Sato and R. Noyori, J. Am. Chem. Soc., 112 (1990) 4897; (c) K. Tani, Pure Appl. Chem., 57 (1985) 1845.
2 (a) M. Kitamura, T. Ohkuma, M. Tokunaza and R. Noyori, Tetrahedron: Asym., 1 (1990) 1; (b) T. Ohta, H. Takaya and R. Noyori, Inorg. Chem., 27 (1988) 566.
3 C. Ammann, P.S. Pregosin, H. Rüegger, M. Grassi and A. Musco, Magn. Reson. Chem., 27 (1989) 355.
4 P.S. Pregosin and C. Ammann, Pure Appl. Chem. 61 (1989) 1771.
5 M. Grassi, S.V. Meille, A. Musco, R. Pontellini and A. Sironi, J. Chem. Soc., Dalton Trans., (1990) 251 and (1989) 615.
6 K. Miki, K. Yamatoya, N. Kasai, H. Rusowawa, A. Urabe, M. Emoto, K. Tatsumi and A. Nakamura, J. Am. Chem. Soc., 110 (1988) 3191.
7 G. Facchin, R. Bertoni, M. Calligaris, G. Nardin and M. Mari, J. Chem. Soc., Dalton Trans., (1987) 1381.
8 A. Albinati, R.W. Kunz, C. Ammann and P.S. Pregosin, Organometallics, 10 (1991) 1800.
9 B. Åkermark, B. Krakenberger, S. Hansson and A. Vitagliano, Organometallics, 6 (1987) 620.
10 ^{1}H shifts in allyl ligands can vary widely, see K. Vrieze, H.C. Volger and P.S.N.M. van Leeuwen, Inorg. Chim. Acta Rev., (1969) 109.
11 B.M. Trost, P.E. Strege, L. Weber, T.J. Fullerton and T.J. Dietsche, J. Am. Chem. Soc., 100 (1978) 3407.

12 H. Rüegger, R.W. Kunz, C.J. Ammann and P.S. Pregosin, Magn. Reson. Chem., 29 (1991) 197.
13 A.J. Deeming, T.P. Rothwell, M.B. Hursthouse and J.D.J. Backer Dirks, J. Chem. Commun., (1979) 670.
14 P.K. Byers, A.J. Canty, B.W. Skelton and A.H. White, J. Chem. Soc., Chem. Commun., (1986) 1722.
15 A.J. Deeming, I.P. Rothwell, M.B. Hursthouse and L. New, J. Chem. Soc., Dalton Trans., (1978) 1490.
16 A.J. Deeming, I.P. Rothwell, M.B. Hursthouse and K.M.A. Malik, J. Chem. Soc., (1979) 1899.
17 J.E. Gozum, D.M. Pollina, J.A. Jensen and G.S. Girolami, J. Am. Chem. Soc., 110 (1988) 2688.
18 A.E. Smith, Acta Crystallogr., 18 (1965) 331.
19 F.R. Hartley, The Chemistry of Platinum and Palladium, Applied Science Publishers, London, 1973, p. 430.
20 H.C. Clark, M.J. Hampden-Smith and H. Rüegger, Organometallics, 7 (1988) 2085 and references quoted therein.
21 Y. Hayashi, K. Matsumoto and Y. Nakamura, J. Chem. Soc., Dalton Trans., (1989) 1519.
22 H. Rüegger, Magn. Reson. Chem., 29 (1991) 113.
23 Ring current effects are well known, see F.A. Bovey, Nuclear Magnetic Resonance Spectroscopy, Academic Press, New York, 1969 and J.W. Akitt, NMR and Chemistry, second edition, Chapman & Hall, London, 1987.
24 K. Toriumi, T. Ito, H. Takaya, T. Souchi and R. Noyori, Acta Cryst., B38 (1982) 807.
25 K. Mashima, K. Kusano, T. Ohta, R. Noyori and H. Takaya, J. Chem. Soc., Chem. Commun., (1989) 466.
27 P.M. Maitlis, P. Espinet and M.J.H. Russel, in G. Willemson, F.G.A. Stone and E. Abel (Eds.), Comprehensive Organometallic Chemistry, Vol. 6, Pergamon, Oxford, 1982, p. 385.
28 N.L. Allinger, MM2(87), Quantum chemistry program exchange, Indiana University.
29 Enraf–Nonius Structure Determination Package, SDP Enraf–Nonius: Delft, Holland (1986).
30 International Tables for X-ray Crystallography, Vol. 4, The Kynoch Press; Birmingham, England, 1974.
31 W.C. Hamilton, Acta Crystallogr., 13 (1965) 502.
32 D. Rogers, Acta Crystallogr., Sect. A, 37 (1981) 734.
33 V. Sklener, H. Miyashiro, G. Zon, H.T. Miles and A. Bax, FEBS Lett., 208 (1986) 94.
34 M.F. Summers, L.G. Marzilli and A. Bax, J. Am. Chem. Soc., 108 (1986) 4285.
35 J. Jeener, G.H. Meier, P. Bachmann and R.R. Ernst, J. Chem. Phys., 71 (1979) 4546.